



Cite this: *Chem. Sci.*, 2021, **12**, 6442

All publication charges for this article have been paid for by the Royal Society of Chemistry

Received 7th February 2021  
Accepted 30th March 2021

DOI: 10.1039/d1sc00752a  
[rsc.li/chemical-science](http://rsc.li/chemical-science)

## Introduction

Nitric acid is an industrially important compound. It is largely used to make nitrate-based fertilizers that are essential for food production from plants.<sup>1,2</sup> Without the use of fertilizers it would be impossible to feed the 8 billion human population on earth. Nitric acid used as a basis for nitrate fertilizers is manufactured by oxidizing ammonia using the Ostwald process (Fig. 1), and the ammonia used here comes primarily from the Haber–Bosch (HB) process ( $N_2 + 3H_2 \rightarrow 2NH_3$ ).<sup>3,4</sup> Unfortunately this process requires harsh reaction conditions ( $P \sim 150$  atm and  $T \sim 700$  K) and it is highly energy intensive, using  $\sim 1\%$  of the total global energy consumption. The process has a high carbon-footprint since one of the reactants,  $H_2$ , comes primarily from the steam reforming process where fossil resources react with water to form  $H_2$  and  $CO_2$  (Fig. 1). Approximately 1.9 metric tons of  $CO_2$  is formed per metric ton of  $NH_3$  produced which contributes significantly to the climate change.<sup>5,6</sup> Hence, it is highly desirable to bypass the ammonia route and develop a direct and sustainable method for  $N_2$  fixation such as alternative routes to nitric acid formation.<sup>7</sup>

Direct oxidation of molecular nitrogen provides a moderately endothermic approach to produce nitrogen oxides and, ultimately, nitric acid (Fig. 1).<sup>9,10</sup> The reaction is however extremely slow at ambient conditions<sup>11</sup> – a good thing in general, since it helps maintain low concentration of  $NO_x$  and nitric acid in our ecosystem. Only very high temperatures or plasmas enable reasonable reaction rates.<sup>12–19</sup>

Center for Catalysis Theory, Technical University of Denmark, Fysikvej Building 311, 2800 Kongens Lyngby, Denmark. E-mail: [jkno@dtu.dk](mailto:jkno@dtu.dk)

† Electronic supplementary information (ESI) available. See DOI: [10.1039/d1sc00752a](https://doi.org/10.1039/d1sc00752a)

## Electrochemical oxidation of molecular nitrogen to nitric acid – towards a molecular level understanding of the challenges†

Megha Anand, Christina S. Abraham and Jens K. Nørskov \*

Nitric acid is manufactured by oxidizing ammonia where the ammonia comes from an energy demanding and non-eco-friendly, Haber–Bosch process. Electrochemical oxidation of  $N_2$  to nitric acid using renewable electricity could be a promising alternative to bypass the ammonia route. In this work, we discuss the plausible reaction mechanisms of electrochemical  $N_2$  oxidation (N<sub>2</sub>OR) at the molecular level and its competition with the parasitic oxygen evolution reaction (OER). We suggest the design strategies for  $N_2$  oxidation electro-catalysts by first comparing the performance of two catalysts –  $TiO_2(110)$  (poor OER catalyst) and  $IrO_2(110)$  (good OER catalyst), towards dinitrogen oxidation and then establish trends/scaling relations to correlate OER and N<sub>2</sub>OR activities. The challenges associated with electrochemical N<sub>2</sub>OR are highlighted.

Electrochemical oxidative fixation of molecular nitrogen (Fig. 1) appears to be a very attractive approach to drive the endothermic reaction at ambient conditions, where the electricity needed can come from the renewable energy sources making the process sustainable. The reaction has an equilibrium potential of 1.32 eV and previous reports suggest that at pHs above 1.3, the formation of nitrate ions is thermodynamically favoured over the parasitic oxygen evolution reaction for a wide range of potentials.<sup>6</sup>

There is a general lack of natural or artificial electro-catalysts for dinitrogen oxidation.<sup>20</sup> Recently, a few experimental reports emerged suggesting Pd-decorated MXenes and several oxides as potential electrocatalysts for nitrogen oxidative fixation.<sup>21–24</sup>

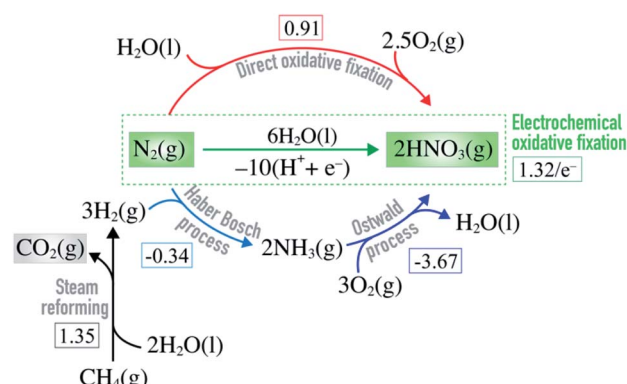


Fig. 1 Equations showing how nitric acid is manufactured on industrial scale by combining steam reforming, Haber–Bosch and Ostwald processes. Direct and electrochemical oxidative  $N_2$  fixation are alternative routes to nitric acid formation. The square brackets contain the free energy of each reaction (in eV) at standard conditions.<sup>8</sup>



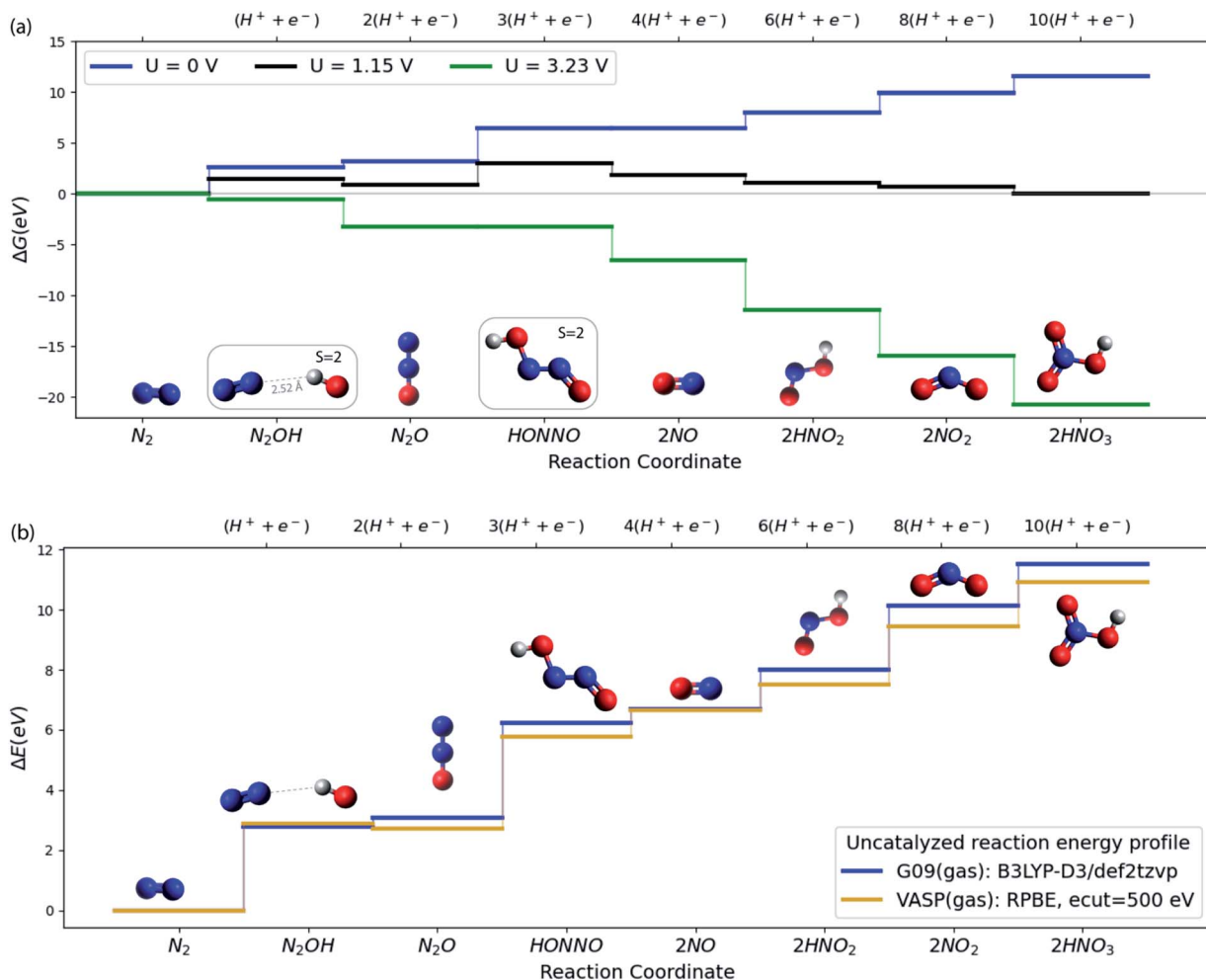


Fig. 2 (a) Free energy plot at SMD( $\text{H}_2\text{O}$ )/B3LYP-D3/def2tzvp level of theory for  $\text{N}_2$  to  $\text{HNO}_3$  conversion. All the relative free energies ( $\Delta G$ ) are evaluated with respect to  $\text{N}_2(\text{g})$ ,  $\text{H}_2(\text{g})$  and  $\text{H}_2\text{O}(\text{l})$ . The blue, black and green lines refer to the 0, equilibrium (1.15 V) and the limiting (3.23 V) potentials respectively. (b) Comparison of VASP and G09 energies of the  $\text{N}_2\text{OR}$  reaction intermediates in vacuum.

There are numerous reports of oxide photo-catalysts for the  $\text{N}_2$  oxidation reaction, prominent among these is  $\text{TiO}_2$ , but there is also a great deal of controversy in that field, see ref. 10 for a recent thorough review.

In the present paper, we aim at contributing to the theoretical framework for understanding the electrochemical dinitrogen oxidation reaction ( $\text{N}_2\text{OR}$ ). The goal is to provide design strategies for  $\text{N}_2\text{OR}$  electro-catalysts both in terms of reaction rates and selectivity towards  $\text{N}_2$  oxidation relative to water oxidation (the oxygen evolution reaction, OER). Building on the work of Medford *et al.*,<sup>25,26</sup> we first discuss the role of a catalyst in terms of stabilization of key intermediates on the basis of a set of density functional theory (DFT) computations. We contrast two catalysts, a good OER catalyst,  $\text{IrO}_2$ , and a poor OER catalyst,  $\text{TiO}_2$ . We then identify several possible rate- and selectivity-determining elementary steps and evaluate the corresponding activation energies.

As a starting point, consider in Fig. 2a the free energy diagram for a set of intermediates defining the simplest possible pathway for  $\text{N}_2$  oxidation in solution. At the SMD( $\text{H}_2\text{O}$ )/

B3LYP-D3/def2tzvp level of theory used here (see ESI†/Computational methods section for details), the free energy for this 10-electron electrochemical reaction is 11.5 eV in reasonable agreement with experiment (12.7 eV) when  $\text{N}_2(\text{g})$ ,  $\text{H}_2(\text{g})$  and  $\text{H}_2\text{O}(\text{g})$  are used as the references at standard conditions.<sup>8</sup> The energetics and the characteristics of the intermediates all agree well with other DFT functionals and experiment as discussed in the ESI.† Fig. 2a illustrates well the difficulty of oxidizing  $\text{N}_2$ , and the ease of the opposite reaction, reduction of nitrate to form  $\text{N}_2$ .<sup>27,28</sup> Applying a positive potential can reduce the thermodynamic barriers for  $\text{N}_2\text{OR}$ , but a very high limiting potential of 3.23 V (vs. RHE) is needed in order for all reaction steps to become exergonic.

We now turn to discuss the ways in which a catalyst can facilitate the reaction. We will discuss solid catalysts deposited on an electrode. To this end we need a calculational scheme that can treat semi-infinite solid surfaces. We use VASP<sup>29–32</sup> with the RPBE exchange–correlation functional,<sup>33</sup> which is known to provide the best treatment of adsorption properties on solid surfaces<sup>34</sup> (see ESI†/Computational methods section for



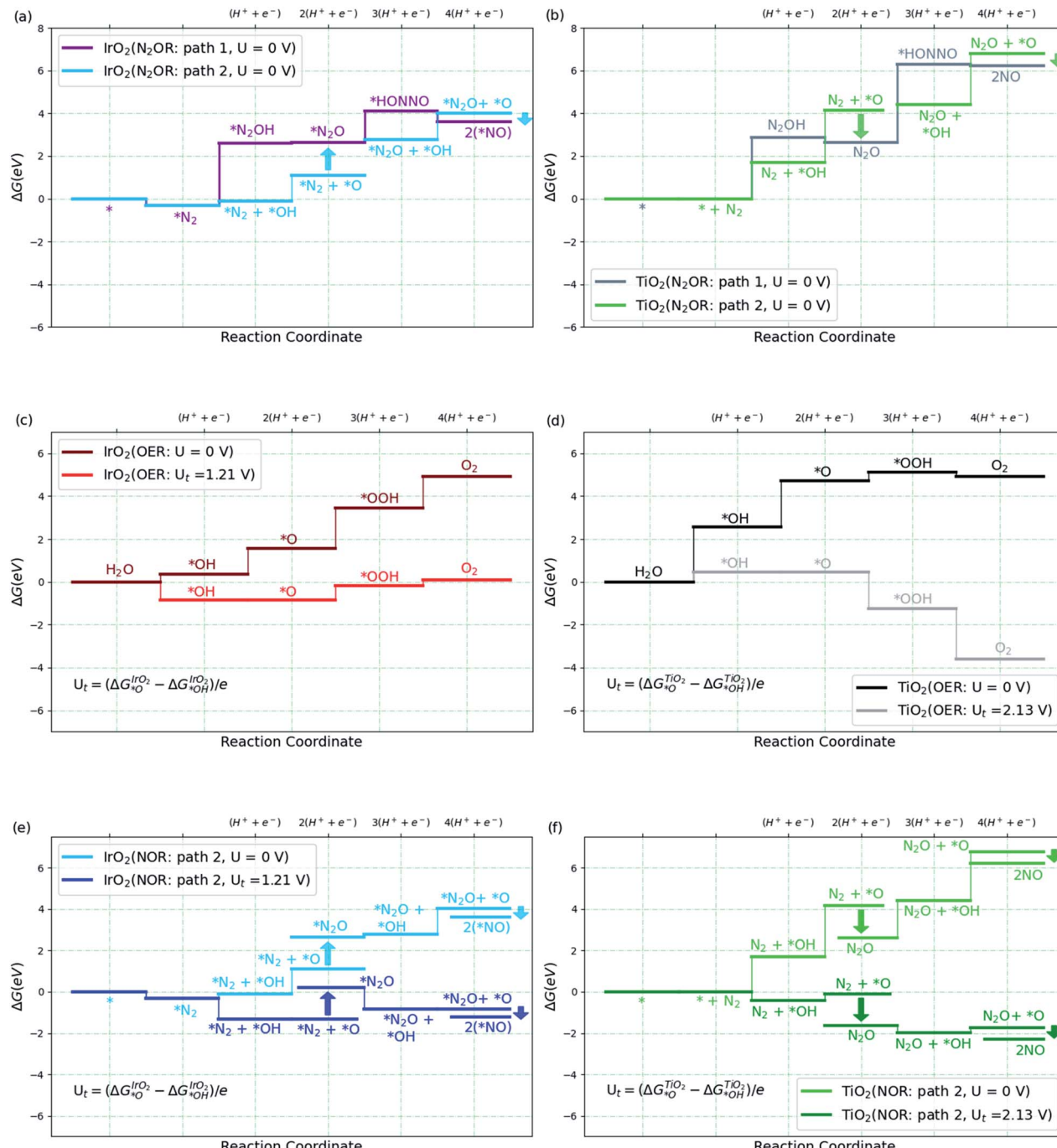


**Fig. 3** (a and b) Free energy diagram for  $N_2$  to NO formation through path 1 and path 2 on  $IrO_2(110)$  and  $TiO_2(110)$ . (c and d) Free energy diagram for oxygen evolution reaction (OER) on high  $*O$  covered  $IrO_2(110)$  and high  $*OH$  covered  $TiO_2(110)$  surfaces at two different potentials,  $U$  and  $U_t$  volts, where  $U_t$  is defined in the plot (see ESI† for coverage details). (e and f) Free energy diagram for  $N_2$  to NO formation via path 2 on  $IrO_2(110)$  and  $TiO_2(110)$  at  $U$  and  $U_t$  volts. The label  $2(*NO)$  refers to 2 times the  $NO-IrO_2(110)$  system. All the relative free energies ( $\Delta G$ ) are evaluated with respect to  $N_2(g)$ ,  $H_2(g)$  and  $H_2O(l)$ .

details). Fig. 2b compares the gas phase energies of reaction intermediates of the uncatalyzed reaction obtained using the RPBE functional in VASP and the B3LYP-D3 functional in Gaussian 09. For the present purposes, the two functionals provide very similar descriptions of the  $N_2$ OR process. In the following sections, we base our treatment of the

electrochemical steps on the RPBE functional. We include entropic terms in the harmonic approximation, (see ESI† for details) in the calculation of the free energies but ignore solvation effects at the surface. We have tested this by studying the electrochemical interface between stoichiometric, defect-free (110) rutile  $TiO_2$  and explicitly adsorbed water in order to

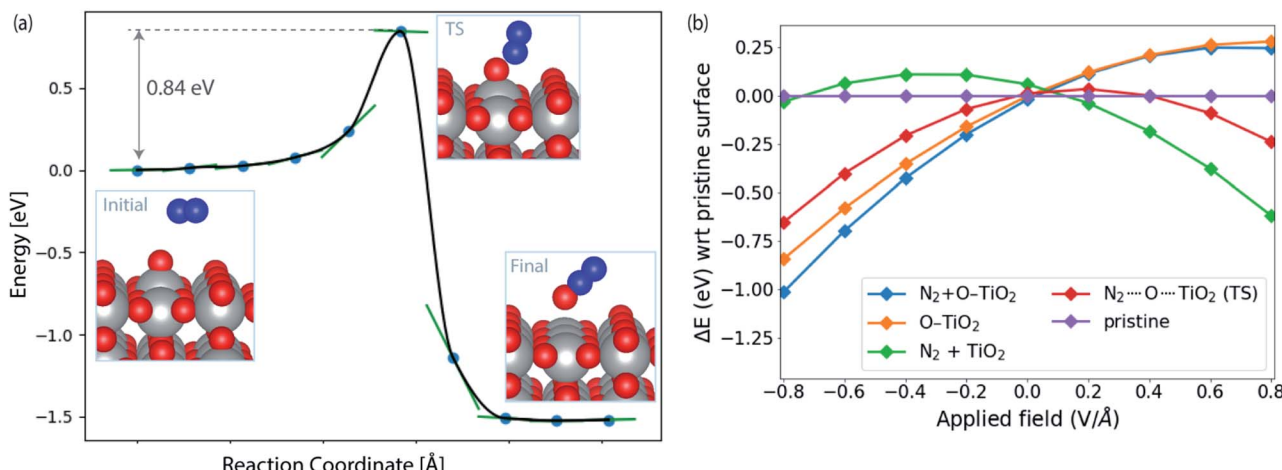


Fig. 4 (a) Reaction pathway and barrier for  $*\text{O} + \text{N}_2 \rightarrow \text{N}_2\text{O}$  formation on  $\text{TiO}_2(110)$ . (b) Influence of applied field on the energies of initial ( $\text{N}_2 + \text{O-TiO}_2$ ) and transition state ( $\text{N}_2\cdots\text{O}\cdots\text{TiO}_2$ ) with respect to the pristine slab ( $\text{TiO}_2(110)$ ). The orange and green lines correspond to the initial structure ( $\text{N}_2 + \text{O-TiO}_2$ ) with  $\text{N}_2$  and  $*\text{O}$  removed from the surface, respectively. See ESI† for details of field computations.

investigate how the presence of water influences the adsorption of the  $\text{N}_2\text{OR}$  intermediates. We find almost no change in the  $\text{N}_2\text{OR}$  adsorbate binding energy with the inclusion of explicit water molecules (see ESI†/Solvation section for more details).

We then consider the reaction over two transition metal oxide surfaces,  $\text{IrO}_2$  and  $\text{TiO}_2$ , both in the rutile structure and in both cases, we consider the (110) facets. Both materials are stable under highly oxidizing conditions, for  $\text{IrO}_2$  at least up to potentials of interest for the oxygen evolution reaction.<sup>9,35–38</sup> Here we focus on the path to producing NO, since the steps following that are relatively facile even at the equilibrium potential, as shown in Fig. 2a. Fig. 3a and b show the free energy diagram for two pathways for the two surfaces. Path 1 is the one we studied in solution (Fig. 2a), while the new path 2, starts with water oxidation to form adsorbed OH as first discussed by Medford and co-workers.<sup>26</sup> The formation of adsorbed OH is less endergonic than the first oxidation step of  $\text{N}_2$  to form adsorbed  $\text{N}_2\text{OH}$  for both surfaces. We therefore concentrate on path 2 in the following sections.

Adsorbed OH (or  $*\text{OH}$ ) can react with  $\text{N}_2$  involving a proton and electron transfer to form  $\text{N}_2\text{O}$  ( $*\text{OH} + \text{N}_2 \rightarrow \text{N}_2\text{O} + \text{H}^+ + \text{e}^-$ ). Alternatively,  $*\text{OH}$  can be oxidized further to form adsorbed O, which can react in two ways. It can form  $\text{O}_2$  by direct recombination or react with water in an electrochemical process to form adsorbed OOH and, after another electron and proton transfer,  $\text{O}_2$ , Fig. 3c and d. This is the usual oxygen evolution reaction. Alternatively, the adsorbed O can react with  $\text{N}_2$  in a non-electrochemical process  $*\text{O} + \text{N}_2 \rightarrow *\text{N}_2\text{O}$ , and further,  $*\text{O} + \text{N}_2\text{O} \rightarrow 2*\text{NO}$  ( $=*\text{N}_2\text{O}_2$ ) (Fig. 3e and f). It can be seen that, as expected, OER is much more facile than  $\text{N}_2\text{OR}$  for  $\text{IrO}_2$ . Indeed, for  $\text{IrO}_2$ ,  $*\text{N}_2\text{O}$  is considerably less stable than  $*\text{O} + *\text{N}_2$  making the  $\text{N}_2\text{OR}$  reaction very slow, while OER becomes facile thermochemically at potentials above 1.5 V. On  $\text{TiO}_2$ , on the other hand, the adsorbed O is so unstable, that  $\text{N}_2\text{O}$  formation is highly exergonic. We therefore discuss  $\text{TiO}_2$  in more detail below.

Most of the reaction steps in Fig. 3e and f involve proton transfers from oxygen to water (in acidic conditions). Such barriers have been found to be very small, of the order 0.2 eV, in studies of water oxidation.<sup>39</sup> We expect the highest barriers to be associated with the activation of  $\text{N}_2$ . For the  $\text{N}_2\text{OR}$  path 2, there are two possible rate determining steps to form  $\text{N}_2\text{O}$ , the electrochemical pathway,  $*\text{OH} + \text{N}_2 \rightarrow \text{N}_2\text{O} + \text{H}^+ + \text{e}^-$  or the purely chemical pathway,  $*\text{O} + \text{N}_2 \rightarrow \text{N}_2\text{O}$ . In the following, we explore the chemical pathway, including the next chemical step,  $*\text{O} + \text{N}_2\text{O} \rightarrow \text{N}_2\text{O}_2 \rightarrow 2*\text{NO}$ .

Fig. 4a shows the calculated activation energy for the reaction  $*\text{O} + \text{N}_2 \rightarrow \text{N}_2\text{O}$  over a  $\text{TiO}_2(110)$  surface. A value of 0.84 eV is found at this level of theory. Outside an electrode surface we need to include electric field effects. It can be seen in Fig. 3f that we need to apply a potential of  $U_t = (\Delta G_O - \Delta G_{\text{OH}})/e$  in order for adsorbed O to become thermodynamically stable at the surface. For  $\text{TiO}_2$ , this value is  $U_t = 2.13$  V. If we assume a width of 3  $\text{\AA}$  for the Helmholtz layer outside the electrode,<sup>40</sup> this corresponds to a field strength of  $E \sim U_t/d \sim 0.7 \text{ V \AA}^{-1}$ , depending

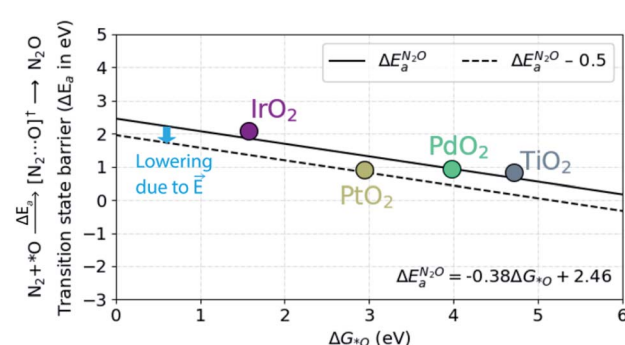


Fig. 5 Scaling relationship between  $\Delta G_O$  and the barrier ( $\Delta E_a$ ) for the  $\text{N}_2\text{O}$  formation. The dotted line includes the 0.5 eV lowering of the barrier due to the local electric field that exists in the electric double-layer at the electrode–electrolyte interface in electrochemical reactions.



on the value of the potential of zero charge of the system. In Fig. 4b we show the energy of adsorbed O and the transition state of  $\text{N}_2\text{O}$  formation as a function of field strength outside a  $\text{TiO}_2(110)$  surface. Clearly  $^*\text{O}$  is strongly destabilized while the transition state is stabilized at positive fields. For  $\text{TiO}_2$ , the net effect is a reduction of the activation energy of the order 0.5 eV. Finally, in order to evaluate the activation free energy, we need to include the loss of gas phase entropy of  $\text{N}_2$  during the reaction. This would add an energy of the order of 0.6 eV to the free energy barrier for the reaction (see ESI† for more details). The net free energy barrier is thus of the order 1 eV according to this very rough estimate.

An activation free energy of the order 1 eV should give a measurable  $\text{N}_2\text{OR}$  rate unless the selectivity is low. Based on the model developed in ref. 39 to estimate the activation energy for OER over  $\text{TiO}_2$ , the activation energy for oxygen evolution is considerably low. Even given the crudeness of the estimate of the free energy barrier for  $\text{N}_2\text{OR}$ , this result strongly suggests that  $\text{N}_2\text{OR}$  through the direct chemical reaction of  $\text{N}_2$  and  $\text{N}_2\text{O}$  with adsorbed O is difficult over  $\text{TiO}_2$ . We cannot rule out that the alternative electrochemical process,  $^*\text{OH} + \text{N}_2 \rightarrow \text{N}_2\text{O} + \text{H}^+ + \text{e}^-$ , will work. That is beyond the present work. We find similar activation barrier of 0.77 eV for the  $\text{N}_2\text{O}_2$  formation ( $^*\text{O} + \text{N}_2\text{O} \rightarrow \text{N}_2\text{O}_2$ ).

In order to understand the trends in the chemical  $\text{N}_2\text{O}$  formation barrier we show in Fig. 5 the variation in the activation energy to form  $\text{N}_2\text{O}$  with the O adsorption energy including additional oxide surface models. There is a strong linear scaling such that a weaker O adsorption bond gives a lower activation energy. A more facile  $\text{N}_2\text{OR}$  process would therefore require a catalyst binding O even weaker than  $\text{TiO}_2$ . The problem is that such a material would still have low activation energy for OER according to the model in ref. 39.

A more promising strategy towards a high selectivity may be to impede the electrochemical oxygen evolution (OER) step relative to the chemical  $\text{N}_2\text{OR}$  steps. This can be accomplished by limiting the access to either proton acceptors or electron acceptors (holes). Limited access to proton acceptors can be accomplished by using a non-aqueous solvent with few proton acceptors. A similar strategy has already been used successfully to increase the selectivity of electrochemical  $\text{N}_2$  reduction (where the parasitic reaction is hydrogen evolution).<sup>41–44</sup> Limited access to holes can for instance be achieved by limiting conductivity to the surface. For  $\text{TiO}_2$  this could be achieved by controlling the thickness of a non-conducting  $\text{TiO}_2$  film on the electrode surface.<sup>45</sup> Limited access to holes could be what is achieved in photochemical  $\text{N}_2\text{OR}$ . We note that any lowering of the electrochemical rates will of course lower the overall rate since the first  $\text{N}_2\text{OR}$  steps are electrochemical.

## Conclusions

In conclusion, we provide a molecular level understanding of the challenges associated with the electrochemical nitrogen oxidation reaction. We analyse the possibility of  $\text{N}_2\text{OR}$  on an excellent OER catalyst,  $\text{IrO}_2(110)$  and a poor OER catalyst  $\text{TiO}_2(110)$ . Obviously OER supersedes  $\text{N}_2\text{OR}$  on  $\text{IrO}_2$  and  $\text{TiO}_2$

turns out to be a borderline  $\text{N}_2\text{OR}$  catalyst. We suggest ways to suppress OER in order to promote  $\text{N}_2\text{OR}$  on oxide surfaces.

## Author contributions

J. K. N. and M. A. conceptualised the paper. M. A. performed all the computations except the aqueous stability computations which were done by C. S. A. All authors contributed towards writing the manuscript.

## Conflicts of interest

There are no conflicts to declare.

## Acknowledgements

This work was supported by the Toyota Research Institute and V-Sustain: The VILLUM Centre for the Science of Sustainable Fuels and Chemicals (9455) from VILLUM FONDEN.

## Notes and references

- 1 J. M. Modak, Haber Process for Ammonia Synthesis, *Resonance*, 2002, 69–77.
- 2 T. Kandemir, M. E. Schuster, A. Senyshyn, M. Behrens and R. Schlögl, The Haber–Bosch Process Revisited: On the Real Structure and Stability of “Ammonia Iron” under Working Conditions, *Angew. Chem., Int. Ed.*, 2013, **52**, 12723–12726.
- 3 K. Wang, D. Smith and Y. Zheng, Electron-driven heterogeneous catalytic synthesis of ammonia: current states and perspective, *Carbon Resour. Convers.*, 2018, **1**, 2–31.
- 4 A. Valera-Medina, H. Xiao, M. Owen-Jones, W. I. David and P. J. Bowen, Ammonia for power, *Prog. Energy Combust. Sci.*, 2018, **69**, 63–102.
- 5 R. Schlögl, Catalytic synthesis of ammonia – a “never-ending story”?, *Angew. Chem., Int. Ed.*, 2003, **42**, 2004–2008.
- 6 J. G. Chen, *et al.* Beyond fossil fuel-driven nitrogen transformations, *Science*, 2018, 360.
- 7 J. Baltrusaitis, Sustainable Ammonia Production, *ACS Sustainable Chem. Eng.*, 2017, **5**, 9527.
- 8 D. D. Wagman, W. H. Evans, V. B. Parker, R. H. Schumm, I. Halow, S. M. Bailey, K. L. Churney and R. L. Nuttall, The NBS tables of chemical thermodynamics properties: selected values for inorganic and C1 and C2 organic substances in SI units, *J. Phys. Chem. Ref. Data*, 1982, 111–518.
- 9 M. Pourbaix, *Atlas of electrochemical equilibria in aqueous solutions*, Tex: National Association of Corrosion Engineers, Houston, Texas, 1974, p. 500.
- 10 A. J. Medford and M. C. Hatzell, Photon-driven nitrogen fixation: current progress, thermodynamic considerations, and future outlook, *ACS Catal.*, 2017, **7**, 2624–2643.
- 11 G. Charlot, *L'analyse qualitative et les réactions en solution*, 1957, pp. 315–321.



12 Y. Wang, A. W. Desilva, G. C. Goldenbaum and R. R. Dickerson, Nitric oxide production by simulated lightning – dependence on current energy and pressure, *J. Geophys. Res.*, 1998, **103**, 19149–19159.

13 B. S. Patil, Q. Wang, V. Hessel and J. Lang, Plasma N<sub>2</sub>-fixation: 1900–2014, *Catal. Today*, 2015, **256**, 49–66.

14 N. Cherkasov, A. O. Ibhodon and P. Fitzpatrick, A review of the existing and alternative methods for greener nitrogen fixation, *Chem. Eng. Process.*, 2015, **90**, 24–33.

15 X. Fan, S. Kang, J. Li and T. Zhu, Formation of nitrogen oxides (N<sub>2</sub>O, NO, and NO<sub>2</sub>) in typical plasma and plasma-catalytic processes for air pollution control, *Water, Air, Soil Pollut.*, 2018, **229**, 351–363.

16 Y. He, Z. Chen, Z. Li, G. Niu and J. Tang, Non-thermal plasma fixing of nitrogen into nitrate: solution for renewable electricity storage?, *Front. Optoelectron.*, 2018, **11**, 92–96.

17 S. Li, J. A. M. Jimenez, V. Hessel and F. Gallucci, Recent progress of plasma-assisted nitrogen fixation research: a review, *Processes*, 2018, **6**, 248–273.

18 P. Lamichhane, R. Paneru, L. N. Nguyen, J. S. Lim, P. Bhartiya, B. C. Adhikari, S. Mumtaz and E. H. Choi, Plasma-assisted nitrogen fixation in water with various metals, *React. Chem. Eng.*, 2020, **5**, 2053–2057.

19 Z. Liu, Y. Tian, G. Niu, X. Wang and Y. Duan, Direct Oxidative Nitrogen Fixation from Air and H<sub>2</sub>O by a Water Falling Film Dielectric Barrier Discharge Reactor at Ambient Pressure and Temperature, *ChemSusChem*, 2021, **14**, 1507–1511.

20 Y. Wang, Y. Yu, R. Jia, C. Zhang and B. Zhang, Electrochemical synthesis of nitric acid from air and ammonia through waste utilization, *Natl. Sci. Rev.*, 2019, **6**, 730–738.

21 W. Fang, C. Du, M. Kuang, M. Chen, W. Huang, H. Ren, J. Xu, A. Feldhoff and Q. Yan, Boosting efficient ambient nitrogen oxidation by a well-dispersed Pd on MXene electrocatalyst, *Chem. Commun.*, 2020, **56**, 5779–5782.

22 C. Dai, Y. Sun, G. Chen, A. C. Fisher and Z. J. Xu, Electrochemical Oxidation of Nitrogen towards Direct Nitrate Production on Spinel Oxides, *Angew. Chem.*, 2020, **59**, 9418–9422.

23 M. Kuang, *et al.* Efficient Nitrate Synthesis *via* Ambient Nitrogen Oxidation with Ru-Doped TiO<sub>2</sub>/RuO<sub>2</sub> Electrocatalysts, *Adv. Mater.*, 2020, 2002189–2002196.

24 S. Han, C. Wang, Y. Wang, Y. Yu and B. Zhang, Electrosynthesis of nitrate *via* the oxidation of nitrogen on tensile strained palladium porous nanosheets, *Angew. Chem., Int. Ed.*, 2021, **133**, 1–6.

25 B. M. Comer, Y.-H. Liu, M. B. Dixit, K. B. Hatzell, Y. Ye, E. J. Crumlin, M. C. Hatzell and A. J. Medford, The Role of Adventitious Carbon in Photo-Catalytic Nitrogen Fixation by Titania, *J. Am. Chem. Soc.*, 2018, **140**, 15157–15160.

26 B. M. Comer and A. J. Medford, Analysis of Photocatalytic Nitrogen Fixation on Rutile TiO<sub>2</sub>(110), *ACS Sustainable Chem. Eng.*, 2018, **6**, 4648–4660.

27 V. Rosca, M. Duca, M. T. De Groot and M. T. M. Koper, Nitrogen Cycle Electrocatalysis, *Chem. Rev.*, 2009, **109**, 2209–2244.

28 M. Duca and M. T. M. Koper, Powering denitrification: the perspectives of electrocatalytic nitrate reduction, *Energy Environ. Sci.*, 2012, **5**, 9726–9742.

29 J. Hafner and G. Kresse, *Ab Initio* Molecular Dynamics for Liquid Metals, *Phys. Rev. B: Condens. Matter Mater. Phys.*, 1993, **47**, 558–561.

30 J. Hafner and G. Kresse, *Ab Initio* Molecular-Dynamics Simulation of the Liquid-Metal-Amorphous-Semiconductor Transition in Germanium, *Phys. Rev. B: Condens. Matter Mater. Phys.*, 1994, **49**, 14251–14269.

31 G. Kresse and J. Furthmüller, Efficiency of *Ab Initio* Total Energy Calculations for Metals and Semiconductors Using a Plane-Wave Basis Set, *Comput. Mater. Sci.*, 1996, **6**, 15–50.

32 G. Kresse and J. Furthmüller, Efficient Iterative Schemes for *Ab Initio* Total-Energy Calculations Using a Plane-Wave Basis Set, *Phys. Rev. B: Condens. Matter Mater. Phys.*, 1996, **54**, 11169–11186.

33 B. Hammer, L. Hansen and J. K. Nørskov, Improved adsorption energetics within density functional theory using revised Perdew–Burke–Ernzerhof functionals, *Phys. Rev. B: Condens. Matter Mater. Phys.*, 1999, **59**, 7413–7421.

34 J. Wellendorff, K. T. Lundgaard, A. Møgelhøj, V. Petzold, D. D. Landis, J. K. Nørskov, T. Bligaard and K. W. Jacobsen, Density functionals for surface science: exchange–correlation model development with Bayesian error estimation, *Phys. Rev. B: Condens. Matter Mater. Phys.*, 2012, **85**, 235149–235172.

35 D.-S. Kong and J.-X. Wu, An Electrochemical Study on the Anodic Oxygen Evolution on Oxide Film Covered Titanium, *J. Electrochem. Soc.*, 2008, **155**, C32.

36 S. Cherevko, S. Geiger, O. Kasian, N. Kulyk, J. P. Grote, A. Savan, B. R. Shrestha, S. Merzlikin, B. Breitbach, A. Ludwig and K. J. Mayrhofer, Oxygen and hydrogen evolution reactions on Ru, RuO<sub>2</sub>, Ir, and IrO<sub>2</sub> thin film electrodes in acidic and alkaline electrolytes: a comparative study on activity and stability, *Catal. Today*, 2016, **262**, 170–180.

37 S. Geiger, O. Kasian, M. Ledendecker, E. Pizzutilo, A. M. Mingers, W. T. Fu, O. Diaz-Morales, Z. Li, T. Oellers, L. Fruchter, A. Ludwig, K. J. Mayrhofer, M. T. Koper and S. Cherevko, The stability number as a metric for electrocatalyst stability benchmarking, *Nat. Catal.*, 2018, **1**, 508–515.

38 Z. Wang, X. Guo, J. Montoya and J. K. Nørskov, Predicting aqueous stability of solid with computed Pourbaix diagram using SCAN functional, *npj Comput. Mater.*, 2020, **160**, 1–7.

39 C. F. Dickens, C. Kirk and J. K. Nørskov, Insights into the electrochemical oxygen evolution reaction with *ab initio* calculations and microkinetic modeling: beyond the limiting potential volcano, *J. Phys. Chem. C*, 2019, **123**, 18960–18977.

40 G. S. Karlberg, J. Rossmeisl and J. K. Nørskov, Estimations of electric field effects on the oxygen reduction reaction based on the density functional theory, *Phys. Chem. Chem. Phys.*, 2007, **9**, 5158.



41 A. Tsuneto, A. Kudo and T. Sakata, Efficient Electrochemical Reduction of N<sub>2</sub> to NH<sub>3</sub> catalyzed by Lithium, *Chem. Lett.*, 1993, 851–854.

42 A. Tsuneto, A. Kudo and T. Sakata, Lithium-mediated electrochemical reduction of high pressure N<sub>2</sub> to NH<sub>3</sub>, *J. Electroanal. Chem.*, 1994, 367, 851–854.

43 S. Z. Andersen, M. J. Statt, V. J. Bukas, S. G. Shapley, J. B. Pedersen, K. Krempl, M. Saccoccio, D. Chakraborty, J. Kibsgaard, P. C. K. Vesborg, J. Nørskov and I. Chorkendorff, Increasing stability, efficiency, and fundamental understanding of lithium-mediated electrochemical nitrogen reduction, *Energy Environ. Sci.*, 2020, 13, 4291–4300.

44 N. Lazouski, M. Chung, K. Williams, M. L. Gala and K. Manthiram, Non-aqueous gas diffusion electrodes for rapid ammonia synthesis from nitrogen and water-splitting derived hydrogen, *Nat. Catal.*, 2020, 3, 463–469.

45 V. Viswanathan, K. L. Pickrahn, A. C. Luntz, S. F. Bent and J. K. Nørskov, Nanoscale limitations in metal oxide electrocatalysts for oxygen evolution, *Nano Lett.*, 2014, 14, 5853–5857.

